Supplementary materials for

Unexpected Interfacial Mo-rich Phase in 2D Molybdenum Disulfide and 3D Gold Heterojunctions

Mengjia Wang[a], Ruichun Luo[b], Yuxin Liu[c], Xiaoran Zhao[a], Xiaodong Zhuang[d], Wen Wu Xu[c], Mingwei Chen[e]*, Pan Liu[a]**

[a] Shanghai Key Laboratory of Advanced High-temperature Materials and Precision Forming, State Key Laboratory of Metal Matrix Composites, School of Materials Science and Engineering, Shanghai Jiao Tong University, Shanghai 200240, P. R. China

[b] School of Physical Sciences and CAS Key Laboratory of Vacuum Physics, University of Chinese Academy of Sciences, Beijing 100049, China

[c] Department of Physics, School of Physical Science and Technology, Ningbo University, Ningbo 315211, China

[d] School of Chemistry and Chemical Engineering, Shanghai Jiao Tong University, Shanghai 200240, P. R. China

[e] Department of Materials Science and Engineering, Johns Hopkin University, Baltimore, MD 21218, USA.

*Email address: xuwenwu@nbu.edu.cn, mwchen@jhu.edu, panliu@sjtu.edu.cn

Experimental section

Preparation of Mo–Au surface alloy. NPG sheets with a thickness of 400 nm were prepared by chemically etching $Ag_{65}Au_{35}$ (at%) leaves in a 70 vol% HNO_3 solution (Aldrich) at room temperature for 6 h. After removal of the residual Ag, the NPG sheet was placed on a Si/SiO_2 wafer. $Mo(CO)_6$ (Sigma–Aldrich, purity >99.5%) and S (Aldrich, purity of 99.9%, 3 mg) powders were used as precursors. The samples were prepared using a three-zone tubular furnace under atmospheric pressure conditions. First, 500 sccm Ar flushed the chamber for 30 min to remove oxygen from the tube. NPG sheets were placed downstream of the furnace, and $Mo(CO)_6$ was placed in the furnace center. Subsequently, the NPG sheets were heated to 573 K, and $Mo(CO)_6$ was heated to 363 K under 150 sccm Ar and annealed for 30 min.

Synthesis of molybdenum sulfide and the Mo-rich phase. The Mo-Au surface alloy was heated to 973 K for 20 min. Simultaneously, the S powder (0.3 g or 1 g) placed upstream was heated to 483 K, and the miscible Mo-Au surface alloy was exposed to S vapor for 3 min under 100 sccm Ar and 10 sccm H_2. Then, the sample was rapidly cooled to room temperature.

Material characterization. The HAADF-STEM images were captured by a JEOL ARM 200F TEM (accelerating voltage, 200 kV), which equipped with a cold emission gun and an aberration corrector for the probe-forming lens system. The collection angle of the HAADF detector ranges from 81 to 228 mrad. The filtered HAADF-STEM images were deconvoluted using the HREM DeConvHAADF software. The element concentration at the interface was determined by EDS detector. The EELS spectra were collected with the Gatan GIF Quantum system on STEM mode. The energy resolution of the EELS system measured from the ZLP is about 0.45 eV and all spectra were acquired with an energy dispersion of 0.025 eV per channel. XPS measurements were carried out by an AXIS Ultra DLD XPS system (Kratos). Raman measurements were performed by a WITec alpha-300 Raman microscope with an objective focused 532 nm excitation source.

Atomic-resolution HAADF-STEM simulation. Simulated HAADF-STEM images were obtained using xHREM software. The thermal diffuse scattering absorption of each element was considered. A defocus value of -5 nm and a specimen thickness of ~5 nm was employed. The 200 kV probe with a probe-forming aperture of 22 mrad was considered to be aberration-free. The HAADF detector has a collection angle from 81 to 228 mrad.

First-principles calculations. First-principles calculations based on DFT were performed by the Vienna Ab initio Simulation Package (VASP) code[1] to investigate the structural relaxations and electronic structures. The DFT-D3 method[2] provides a more clear and physically sound separation of mid- and long-range effects and is also superior for such thermochemical, intramolecular dispersion effects by using specially adapted electronic parts, which was used for calculating the vdW interactions and all calculations took the spin-orbit coupling into account. During optimization, all the systems relaxed fully until the energy and force converged to 10^{-5} eV and 10^{-3} eV $Å^{-1}$. To avoid interactions between layers, we set the vacuum space (z direction) as 15 Å. Projector-augmented[3] wave potentials and the exchange-correlation interactions formulated within the Perdew-Burke-Ernzerhof generalized gradient approximation (PBE-GGA)[4] were employed. To sample the first Brillouin zone, the plane-wave cutoff energy was 400 eV, and the product of lattice constants and k points was close to 40.

Supplementary Figures

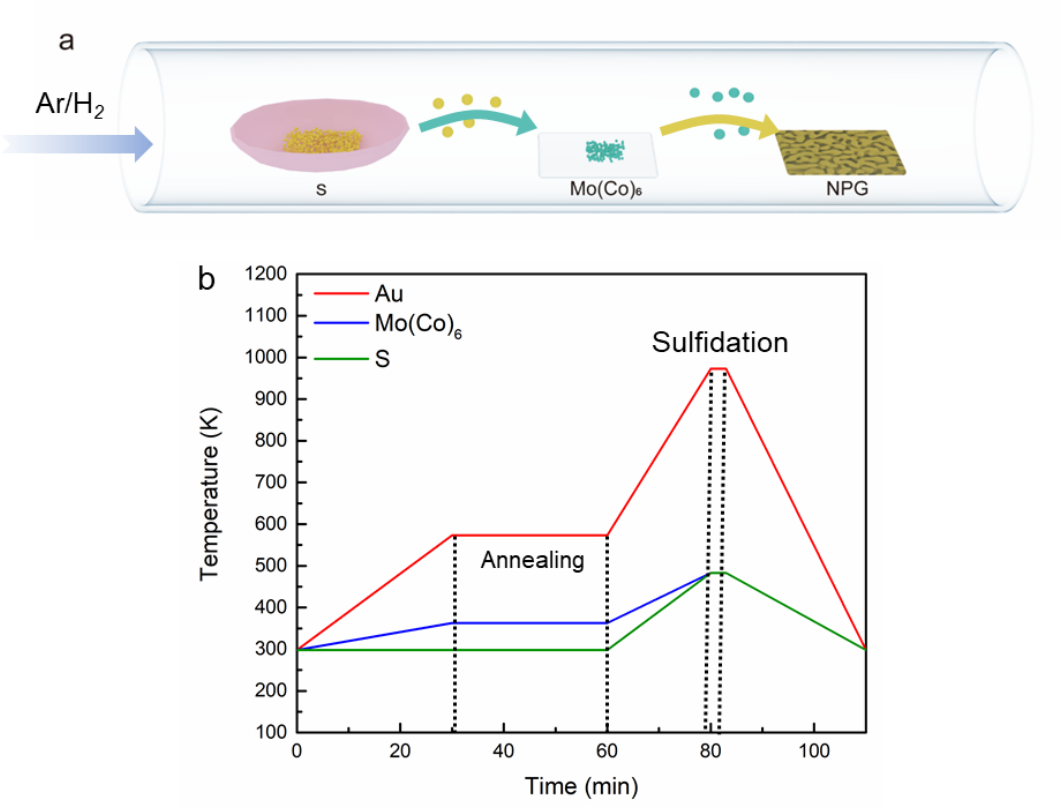

Figure S1. Synthesis process of MoS_2 on NPG by chemical vapor deposition. (a) Schematics of the CVD growth of MoS_2 on NPG. (b) Flow chart of the fabrication procedure.

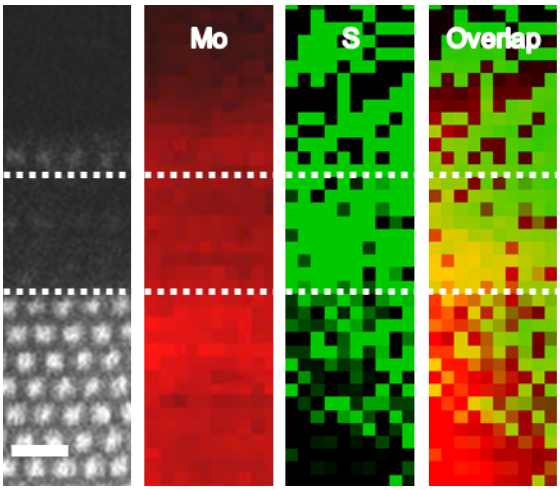

Figure S2. EELS elemental mappings of MoS_2/Au with Mo-rich phase. Scale bar, 0.25 nm.

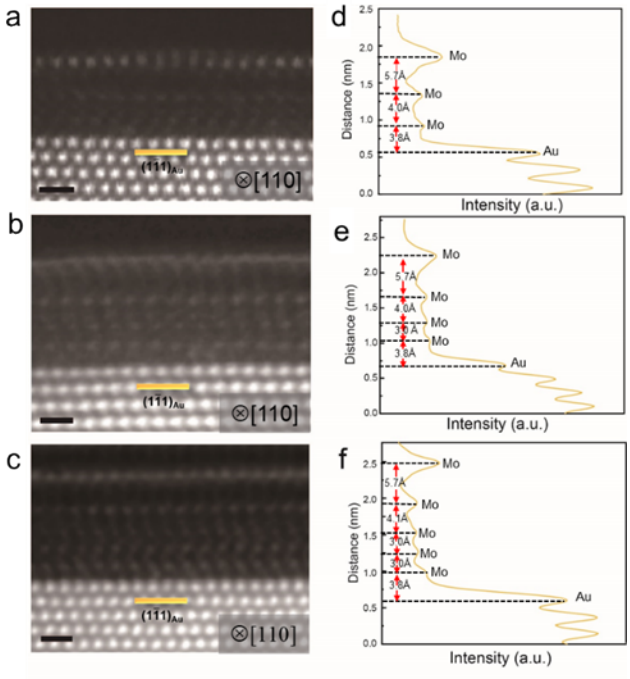

Figure S3. Structural characterizations of the MoS_2/Au interface with Mo-rich phase. (a-c) HAADF-STEM images of MoS_2/Au interface with Mo-rich phase, which is composed of two layers of Mo atoms (a), three layers of Mo atoms (c), four layers of Mo atoms (e). Scale bar,1 nm. (d-f) Corresponding line profile of (a-c).

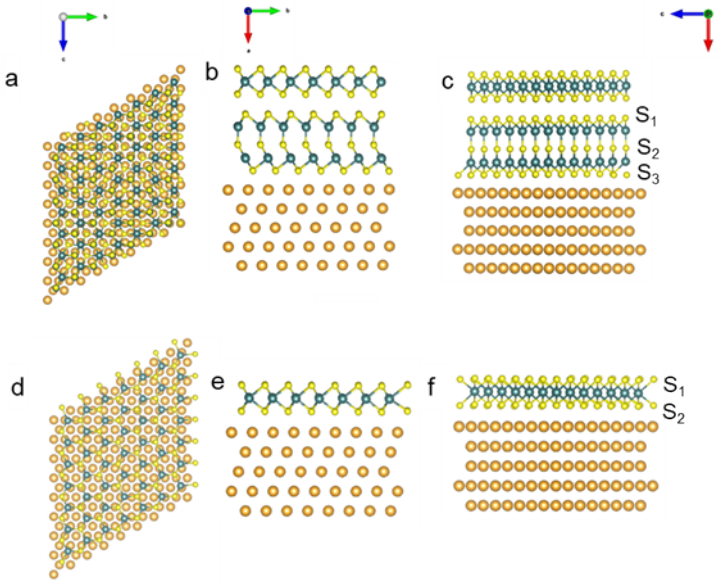

Figure S4. Configuration and orientation relationship of top MoS_2, Mo-rich phase and Au matrix. (a,b) Top and side views the atomic structure of MoS_2/Au heterojunction with Mo-rich phase. (c,d) Top and side views the atomic structure of the MoS_2/Au heterojunction with directly contact. The orange, cyan, and yellow spheres represent Au, Mo, and S atoms, respectively.

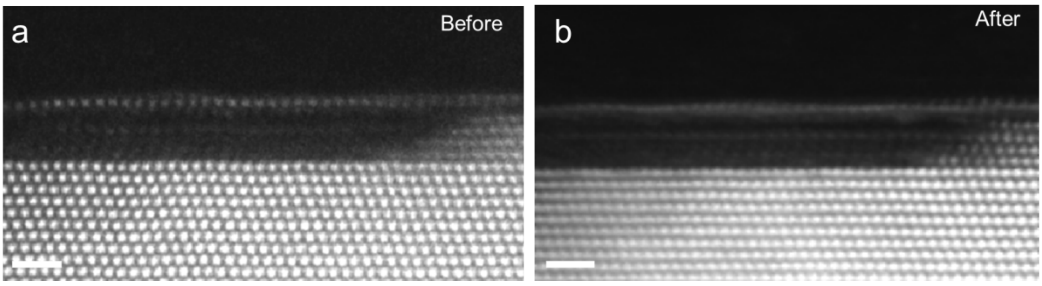

Figure S5. Cross-sectional HAADF-STEM images of MoS_2/Au. (a) Fresh sample; (b) sample after 12 months of exposure to air. Scale bar is 1 nm.

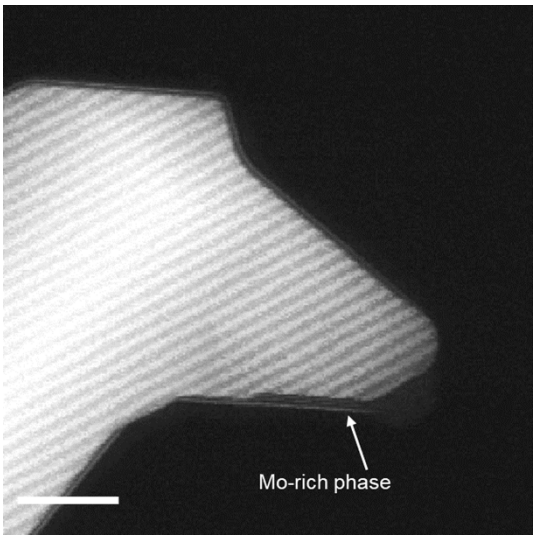

Figure S6. Structure characterization of the MoS_2/Au interface in S-poor environment. Scale bar, 10 nm.

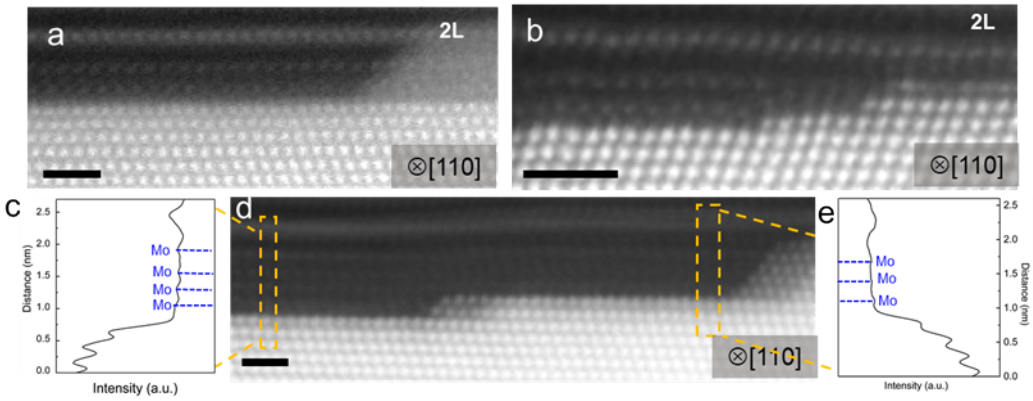

Figure S7. Structure characterization of the MoS_2/Au interface with Mo-rich phase. (a, b) HAADF-STEM image of the MoS_2/Au interface with 2 or 3 layers of Mo-rich phase. (d) HAADF-STEM image of the MoS_2/Au interface with 3 or 4 layers of Mo-rich phase. (c, e) Corresponding line profile extracted from the yellow ellipse in d. ADF-STEM images taken along from the Au [110] direction. Scale bar, 1 nm.

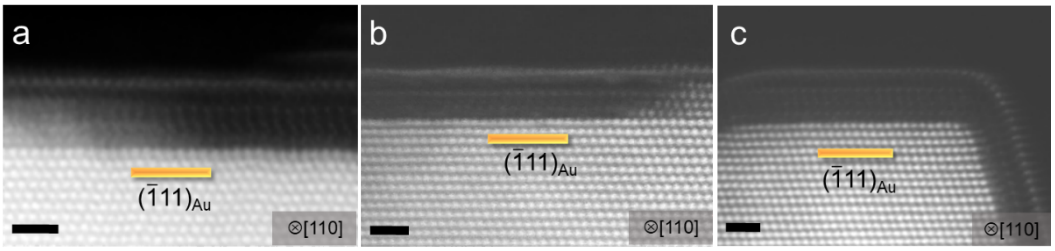

Figure S8. Structural characterizations of the MoS_2/Au interface. The coexistence relationship of the Mo-rich phase and NPG viewed from the $[110]_{Au}$ direction. Scale bar, 1 nm.

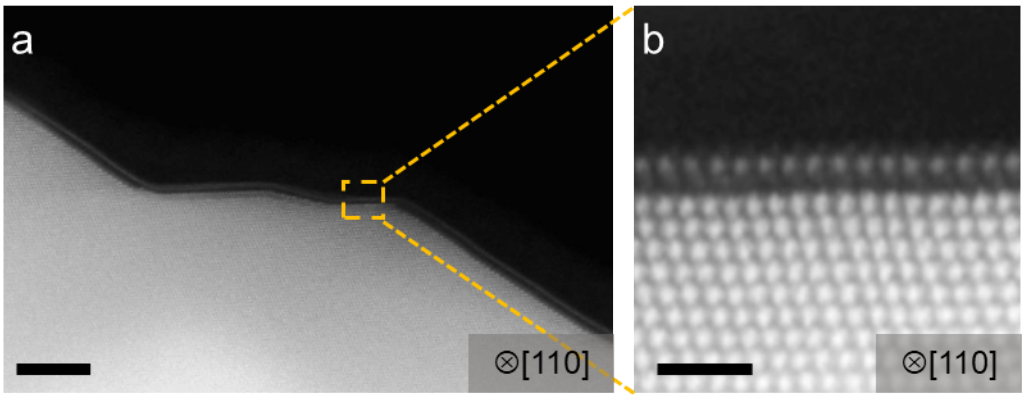

Figure S9. Structure characterization of the MoS_2/Au interface in S-poor environment (S-0.3g). (a) Low magnification HAADF-STEM image of MoS_2/Au interface. Scale bar, 5 nm. (b) Magnified HAADF-STEM image for the yellow ellipse in figure (a). Scale bar, 1 nm. The MoS_2/Au heterointerface is atomically tight, without a second phase or interfacial reconstruction.

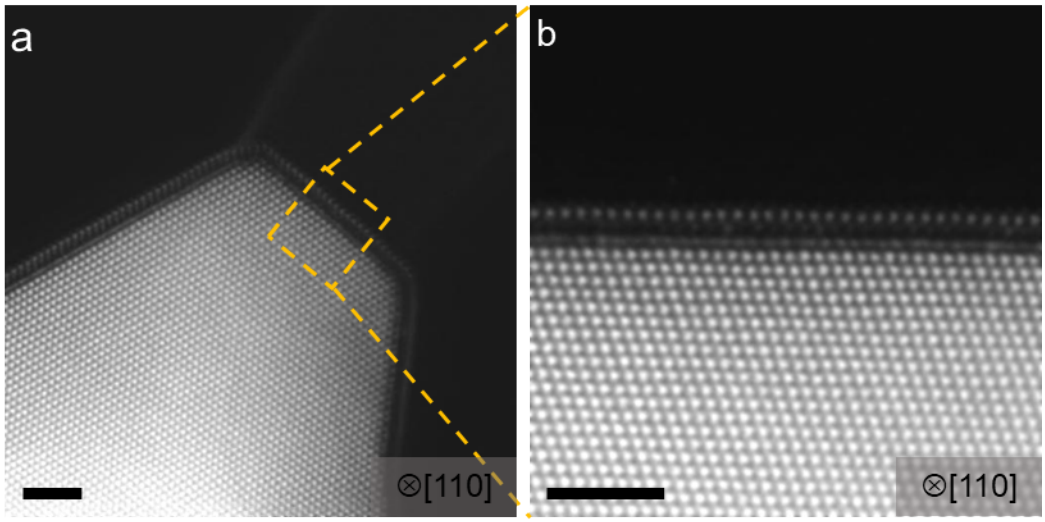

Figure S10. Structure characterization of the MoS_2/Au interface in S-rich environment (S-1g). (a) Low magnification HAADF-STEM image of MoS_2/Au interface. Scale bar, 2 nm. (b) Magnified HAADF-STEM image for the yellow ellipse in figure (a). Scale bar, 1 nm. The excess S leads to the formation of Au-S reconstructed phase at the MoS_2/Au interface.

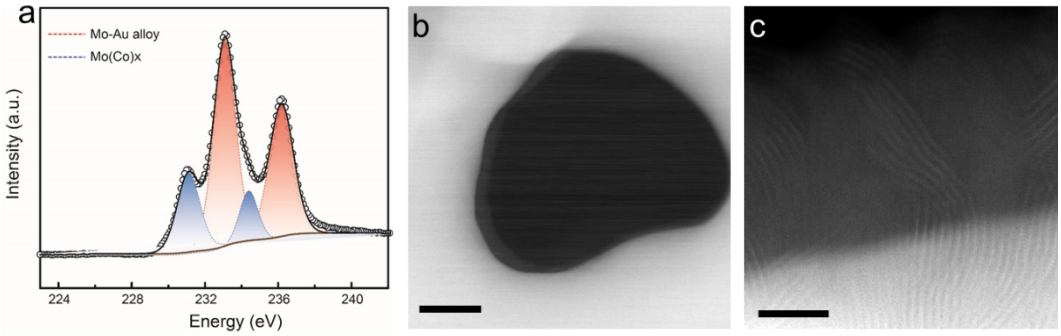

Figure S11. XPS and HAADF-STEM characterization of the Sample with 10 mg $Mo(Co)_6$. (a) XPS for Mo-Au alloy with 10 mg $Mo(Co)_6$. (b) HADDF-STEM of the sample Mo-Au alloy with 10 mg $Mo(Co)_6$. Scale bar, 5 nm. (c) HADDF-STEM image of the Sample after thermal sulfidation with 0.3g S precursor. Scale bar, 1 nm.

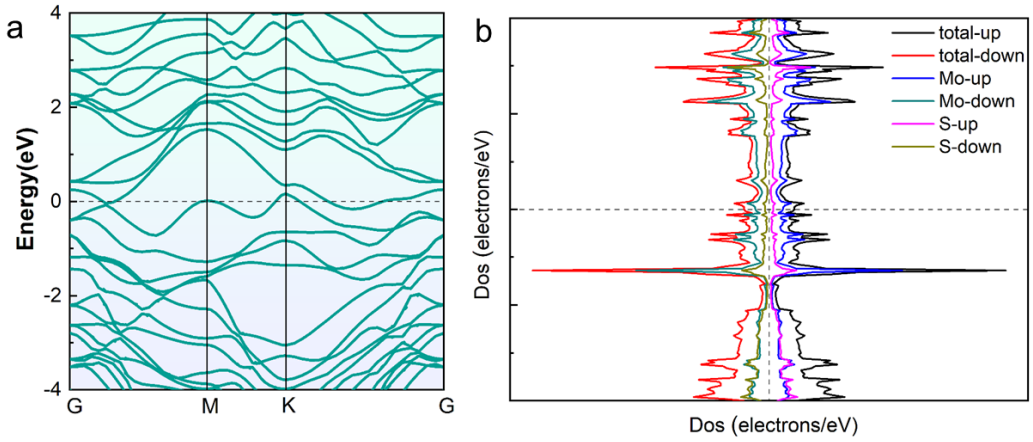

Figure S12. First-principles calculations of Mo-rich phase. (a)The band structure of the Mo-rich phase. (b)Total density of states (DOS), and partial DOS projected on 3d orbits of Mo and 2p orbits of S atom in Mo-rich phase. The perpendicular dashed line at 0 eV.

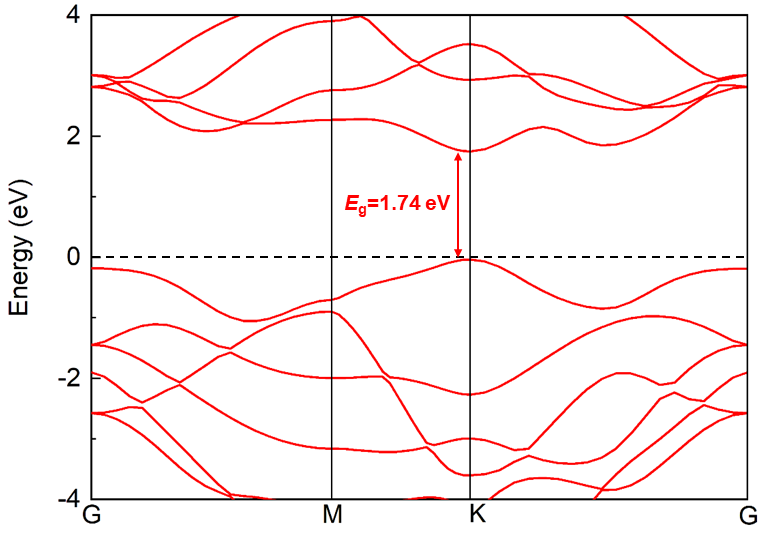

Figure S13. First-principles calculations of the band structure of the monolayer MoS_2. The perpendicular dashed line at 0 eV.

References

1 Giovannetti, G.; Brocks, G.; van den Brink, J. *Phys. Rev. B* 2008, **77**, 035133.

2 Grimme, S.; Antony, J.; Ehrlich, S.; Krieg, H. *J. Chem. Phys*. 2010, **132**, 154104.

3 Blochl, P . E. *Phys. Rev., B Condens. Matter.*1994, **50**, 17953-17979.

4 Perdew J P.; Burke K.; Ernzerhof M. *Phys. Rev. Lett.*1996, **77**, 3865-3868.